Engineered Science
DOI: https://dx.doi.org/10.30919/es1796

Comparative Study of Fluid-Structure Interaction Modeling Techniques Using Solid Elements, Joint-Based Method, and Additional Dead Load in SAP2000

Sarah Eden Suryanto,* Iman Satyarno,* Bambang Supriyadi and Ashar Saputra

Abstract

Fluid-Structure Interaction (FSI) can cause sloshing effects that affect a building's structural response, either positively or negatively. Accurate FSI modeling is essential, especially for structures with swimming pools or water tanks. This study used SAP2000, a Finite Element Method (FEM)-based software, to model FSI through three approaches: Solid Elements, Joint-Based Method, and Additional Dead Load Method. Laboratory tests on a three-story building prototype with a rooftop water tank were used to validate the analysis. Three tank sizes and seven water height variations were evaluated under sinusoidal sweep dynamic loading. Results showed that damping values significantly influenced FSI modeling, with optimal values ranging from 1.4% to 3.9%, matching experimental shaking table data. The Solid Elements method yielded structural displacement results closest to the experimental data, with average differences of 13.62% and 13.81% lower than the Joint-Based and Additional Dead Load methods, respectively. The latter two methods tended to overestimate the structural response. Additionally, sloshing effects were effectively captured only by the Solid Elements approach. These findings highlight the importance of selecting appropriate modeling techniques to ensure accurate simulation of FSI in building structures.

Keywords: Fluid-structure interaction; Sloshing effect; Solid elements; Joint-based methods; SAP2000.

Received: 21 June 2025; Revised: 08 September 2025; Accepted: 02 October 2025.
Article type: Research article.

1. Introduction

In recent years, spill-out incidents resulting from sloshing effects in rooftop swimming pools of high-rise buildings have occurred in several countries, including Bangkok, Thailand during the 2025 Myanmar Earthquake;[1] Taipei, Taiwan during the 2024 Hualien Earthquake;[2] and Manila, Philippines during the 2019 Philippine Earthquake.[3] These events demonstrate that fluid-structure interaction (FSI) can induce sloshing effects capable of causing spill-out and influencing building responses—both positively and negatively. To analyze the impact of FSI, adequate modeling is essential to ensure the safety of occupants and the structural stability of buildings, especially those containing swimming pools, water tanks, or other elements storing large volumes of water.

Several methods have been used to model FSI, including Smoothed Particle Hydrodynamics (SPH),[4-9] Arbitrary Lagrangian-Eulerian (ALE),[10-12] and Finite Element Method (FEM).[4,13-15] The SPH method treats fluids as discrete particles that possess mass, velocity, pressure, and other properties. In contrast, the ALE approach combines the Lagrangian perspective—where the mesh moves with the material—and the Eulerian perspective—where the mesh remains fixed while the material flows through it. FEM, a mesh-based method, is commonly used as the foundation for structural analysis in buildings.

This study used SAP2000, a commercial software based on the FEM, which allows for integrated modeling of building structures and contained water. Within SAP2000, FSI can be simulated using methods such as the Additional Dead Load and Joint-Based Methods.[16-23] In the Additional Dead Load

Department of Civil & Environmental Engineering, Gadjah Mada University, Yogyakarta, 55281, Indonesia
**Email:* imansatyarno@ugm.ac.id (I. Satyarno);
sarah.eden.s@mail.ugm.ac.id (S. E. Suryanto)

method, water is treated as a static load without fluid behavior, thus excluding FSI. The Joint-Based Method considers water mass as separate impulsive and convective components connected to the structure through flexible links, simulating limited fluid behavior but unable to capture sloshing effects. Despite these limitations, both methods are often used to simplify the modeling of significant water volumes, such as in swimming pools.

To address these limitations, this study investigated the Solid Elements method in SAP2000, which allows more accurate representation of sloshing effects.[24] Before applying this method to real buildings, validation is essential. Therefore, laboratory tests on a three-story building prototype with a rooftop water tank were used to compare the performance of the Solid Elements, Joint-Based, and Additional Dead Load methods. The tank was modeled in three geometries and seven water height variations. A sinusoidal frequency sweep (5.0 Hz to 0.5 Hz, amplitude 0.015g) was applied to assess structural responses and potential resonance.

2. Research method

The structural model employed in this study was adapted from a previous experimental investigation that utilized a three-story steel building prototype, featuring additional loads on each floor and a water tank positioned on the top floor.[24] Fig. 1 shows a photograph of the laboratory testing setup along with the specifications of the model used in SAP2000. The experiment was conducted in seven stages, beginning with an empty tank and progressing through incremental additions of water, reaching a total of 186.6 kgf (see Table 1). In addition, three variations of tank dimensions were used to examine the influence of water height relative to tank length, expressed as the height-to-length ratio (d/L).

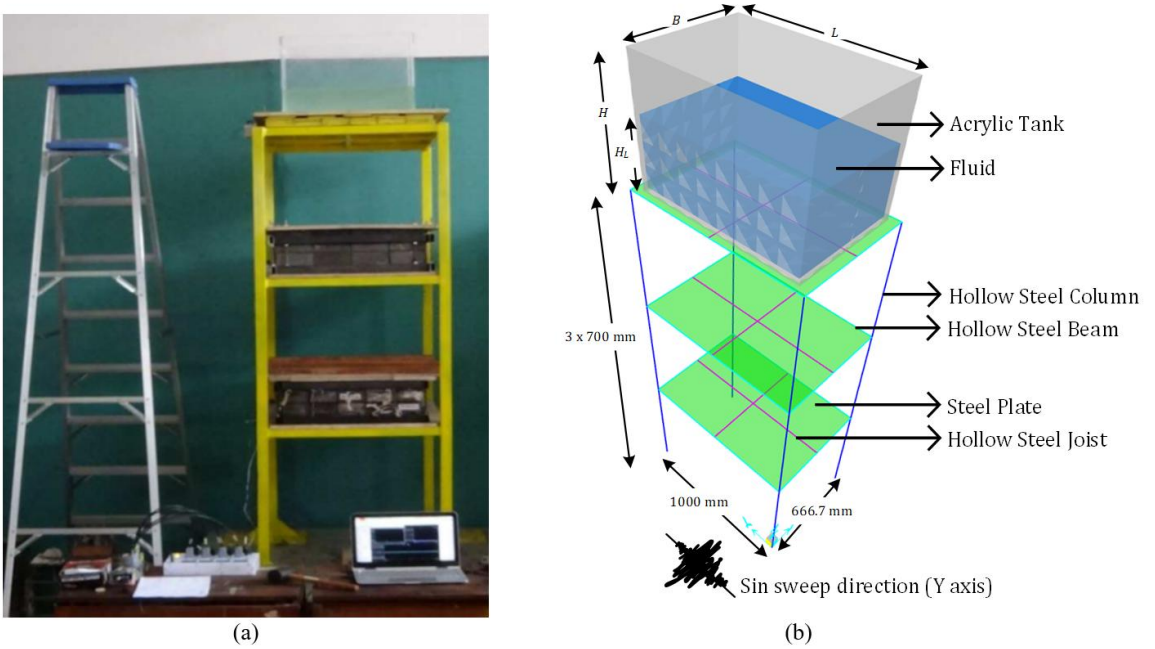

Fig. 1: Experimental structural model (a) and dimensional schematic (b).[9,25]

Table 1: Variations in tank dimensions and corresponding fluid depths.[25]

Step	W_f (kgf)	W_f/W_s (%)	Tank 1 ($B60\times L90\times H60$cm)		Tank 2 ($B60\times L70\times H70$cm)		Tank 3 ($B60\times L50\times H90$cm)	
			d (cm)	d/L	d (cm)	d/L	d (cm)	d/L
1	0	0	0	0	0	0	0	0
2	31.1	2.12	5.76	0.096	7.40	0.123	10.37	0.173
3	62.2	4.24	11.52	0.192	14.81	0.247	20.73	0.346
4	93.3	6.36	17.28	0.288	22.21	0.370	31.10	0.518
5	124.4	8.48	23.04	0.384	29.62	0.494	41.47	0.691
6	155.5	10.60	28.80	0.480	37.02	0.617	51.83	0.864
7	186.6	12.72	34.56	0.576	44.43	0.740	62.20	1.037

Notes: W_f = Weight of fluid; W_s = Weight of structure; d = fluid depth; L = Length of tank.

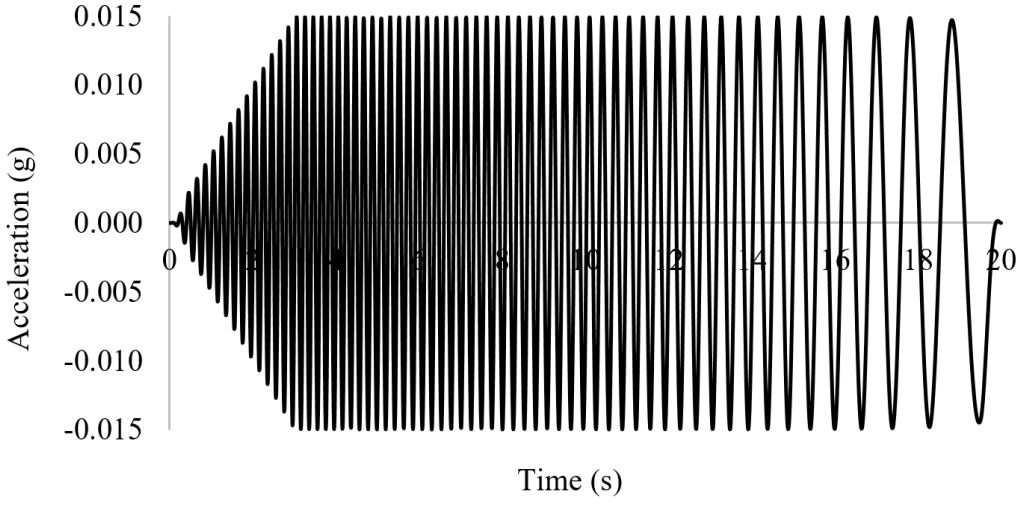

Fig. 2: Sinusoidal sweep excitation with a frequency range of 5.0Hz to 0.5Hz and an amplitude of 0.015g.[9,25]

The experimental testing was conducted on a shaking table, with story dead loads as specified in Table 2, and subjected to a sinusoidal sweep excitation (see Fig. 2). Story dead loads were added to increase the structural weight during laboratory testing. The sinusoidal sweep lasted for 20 seconds, while the structural response was recorded for a total duration of 50 seconds, allowing the structure to undergo free vibration for 30 seconds following the end of excitation.

The overall methodology of creating structural model in SAP2000 is outlined in Fig. 3 and the detail of FSI modeling techniques is shown in Fig. 4. The modeling process began with the creation of structural elements for the column and beam sections, slabs, and water tank, based on the known dimensions. Subsequently, story dead loads ranging from 297.99 kgf to 562.14 kgf were applied to the slab elements on each floor, and the material properties as well as section specifications were defined according to Table 3 and Table 4.

Before proceeding with further analysis, this study performed a control process to address significant variables that may not align with the experimental setup due to limited available information. The first control step involved verifying the consistency between the structural weight in the SAP2000 model (W_{sap}) and that of the experimental model (W_{exp}) (see flowchart in Fig. 3). If W_{sap} did not match W_{exp}, adjustments were made to the mass of structural elements in SAP2000. This study assumed the acrylic tank to behave as a rigid body, and thus, the acrylic tank elements were modeled with constraints.

Once the structural mass was match, the next control step focused on matching the natural frequency in SAP2000 (f_{sap}) with that observed in the laboratory (f_{exp}). If the frequencies differed, adjustments were made to the stiffness of structural elements in SAP2000. This involved modifying the stiffness of hollow columns, beams, and joists without changing the dimension. Following these calibrations, the study proceeded to model FSI using the following three approaches.

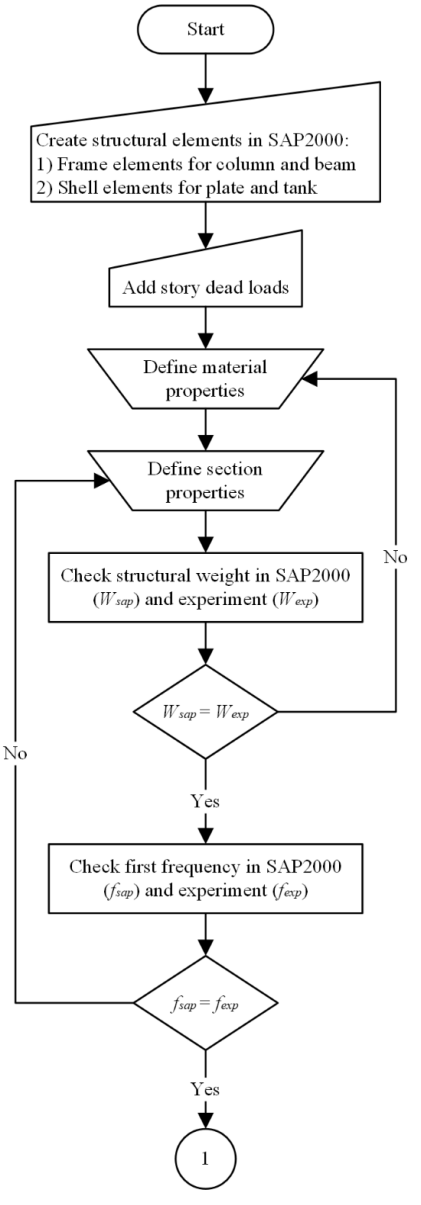

Fig. 3: Procedures of creating basic structural model in SAP2000.

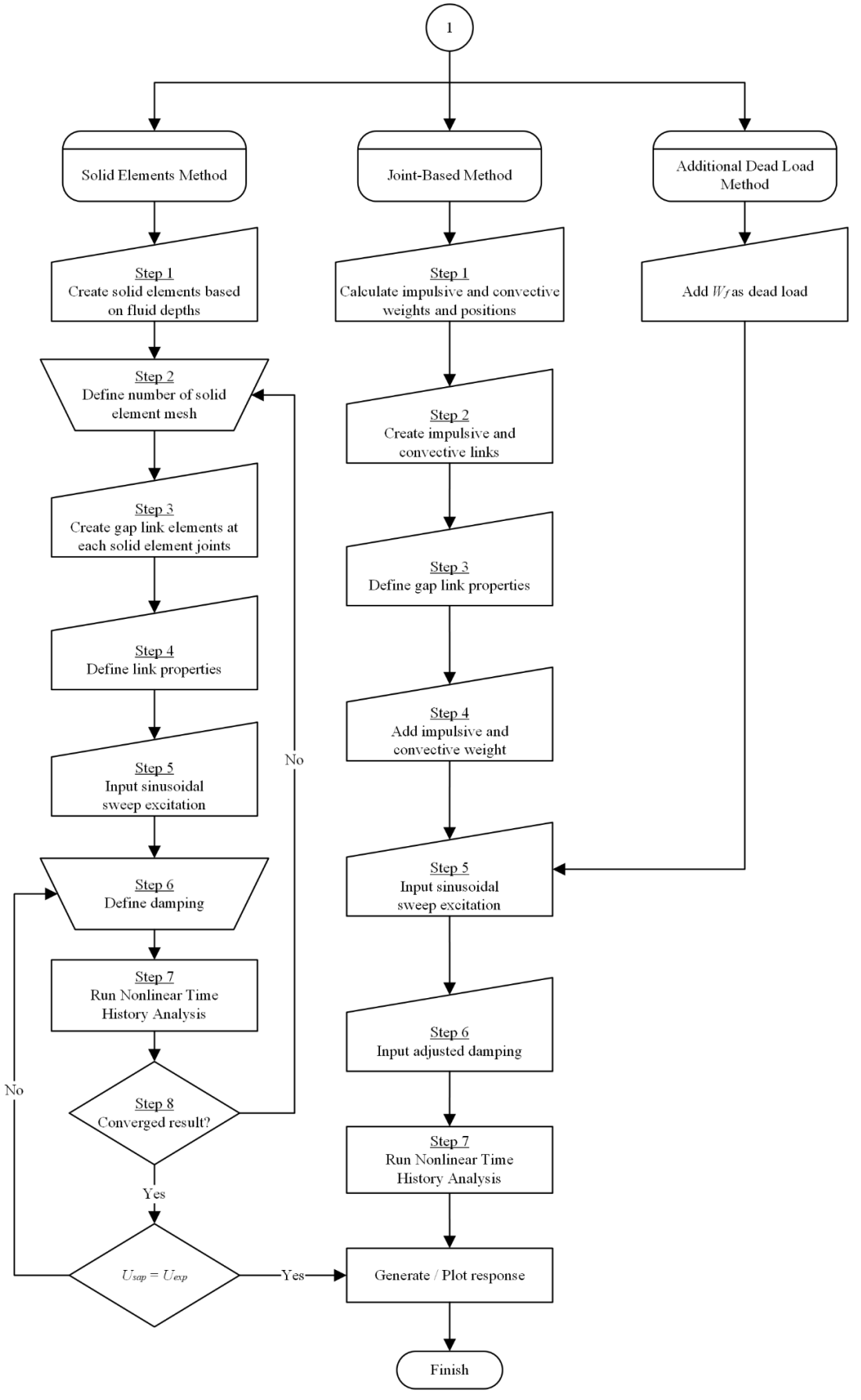

Fig. 4: Procedures of FSI modeling in SAP2000 using the solid elements, joint-based, and additional dead load methods.

Table 2: Story dead load.[25]

Story	Weight of story dead load (W_{SDL}) (kgf)
1	562.14
2	562.14
3	297.99

Table 3: Material properties.[24-27]

No	Material	Mass density (kgf/m^3)	Modulus of elasticity (MPa)
1	Acrylic	1190	2800
2	Steel	7849	200000
3	Fluid	1000	62.05

Table 4: Section properties.[25]

No	Section	Material	Dimension (mm)
1	Hollow column frame	Steel	40 × 40 × 1
2	Hollow beam frame	Steel	40 × 20 × 1.4
3	Hollow joist frame	Steel	20 × 20 × 1.2
4	Plate shell	Steel	1.2
5	Tank shell	Acrylic	10

2.1 Solid elements method

Solid elements are three-dimensional elements consisting of eight nodes and six faces, as illustrated in Fig. 5. These nodes exhibit only translational degrees of freedom, meaning there is no rotational resistance at their connections with other elements such as frame or shell elements. Stresses within the solid element are distributed across its six faces, each subjected to shear stress (τ) and normal stress, either tensile or compressive (σ). In this study, solid elements were utilized to model the water within the tank. The SAP2000 modeling results for the three tank dimension variations are presented in Fig. 6. As previously outlined, the structural models were developed with varying water heights for each tank dimension.

As illustrated in the flowchart in Fig. 4, the second step is to determine the appropriate mesh density for the solid elements. To achieve more accurate results in the solid element analysis, regular quadrilateral mesh types should be employed.[24] Subsequently, step 3 to 4, each node of the solid elements must be connected to other structural elements, such as shell or frame elements. In this model, the solid elements were connected to the shell elements that represent the tank walls. Each node of the solid elements face was linked to the shell elements using a special link element known as a gap link. This link was only applied in the solid elements faces that were connected to the tank walls. Fig. 7 provides a more detailed illustration of the solid element and gap link modeling.

The working principle of the gap link is that it can transfer compressive forces but not tensile ones. This behavior aligns with the physical characteristics of water, which can exert pressure on the tank walls but lacks the capacity to apply tension. The gap links are assigned along the X, Y, and Z directions to facilitate duplication across all joints. However, the characteristics assigned to gap links in each direction are identical: they are allowed to behave nonlinearly in the axial direction (U1) with sufficient stiffness (see Table 5). The gap link in the solid element method is not active in the lateral directions (U2 / U3).

Step 5 applied the sinusoidal sweep excitation to the model. In step 6, the initial damping ratio was set according to the damping value derived from the experimental reference.[25] In SAP2000, proportional damping was applied to the first and second mode frequencies along the direction of excitation. Step 7 run the model by nonlinear time history analysis. If the displacement results in SAP2000 (U_{sap}) did not align with those from the experimental testing (U_{exp}), the damping value was further refined through iterative trial-and-error adjustments (see Step 8). The final adjusted damping values are presented in the following discussion. These adjusted damping values obtained from the solid element method served as the reference for the damping values used in both the joint-based and additional dead load methods.

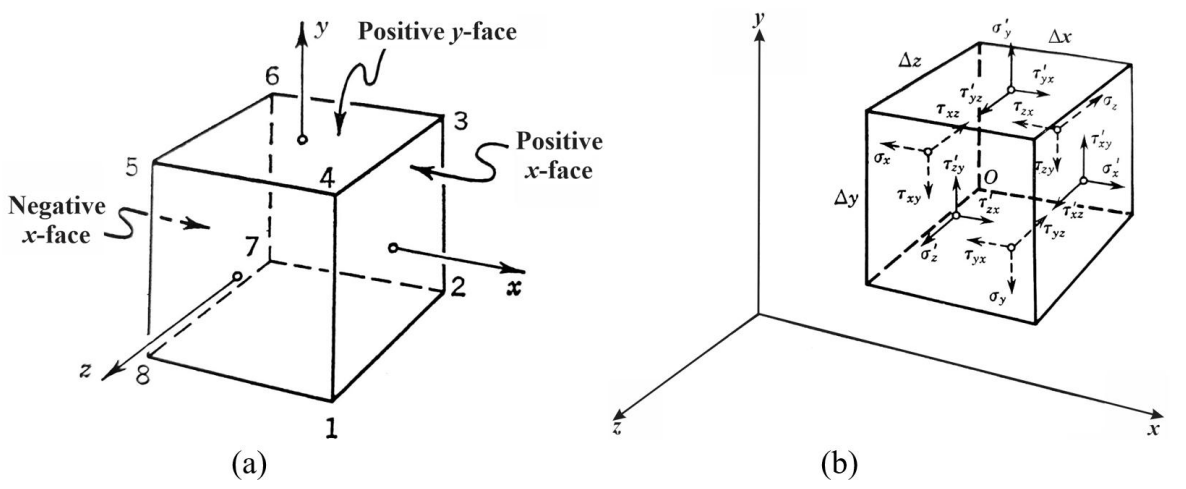

Fig. 5: Definition of solid element nodes and faces (a) as well as stress components acting on the six faces of a parallelepiped (b).[28-30]

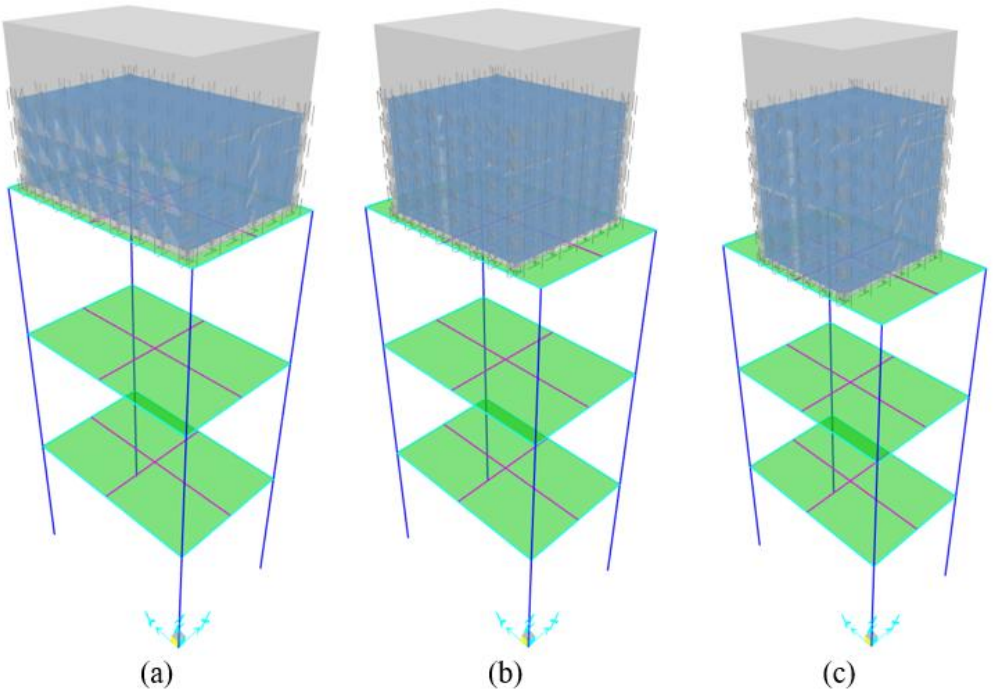

Fig. 6: Structural solid element models in SAP2000 for Tank 1 (a), Tank 2 (b), and Tank 3 (c).

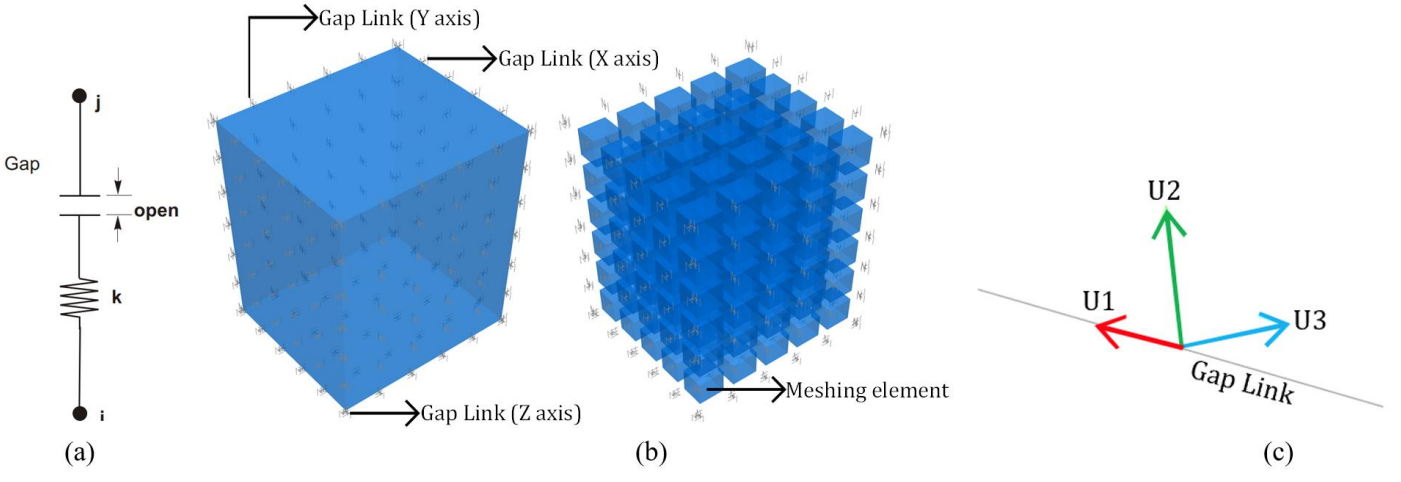

Fig. 7: Theoritical behaviour of gap link (a) as well as its modeling (b) and axis (c) in SAP2000.[26]

Table 5: Gap link characteristic.

Type	U1	U2	U3
Gap link in Solid Element	Nonlinear*	-	-
Gap link in Joint-Based (Impulsive link)	Fix	Fix	-
Gap link in Joint-Based (Convective link)	Nonlinear*	Nonlinear*	-

*The effective stiffness in the nonlinear analysis was assumed to be 10^4 kgf/mm.

2.2 Joint-based method

The fundamental concept of Joint-Based Method involves dividing the fluid mass into two separate components, as shown in Fig. 8. The first component is the impulsive water mass, which moves synchronously with the structure under dynamic loading due to its acceleration being in phase with that of the structure. The second component is the convective water mass, which does not move in unison with the structure. This portion of the fluid can move relatively freely in response to dynamic loads, generating wave effects and additional lateral forces. Therefore, the application of this method also involves the use of gap link.

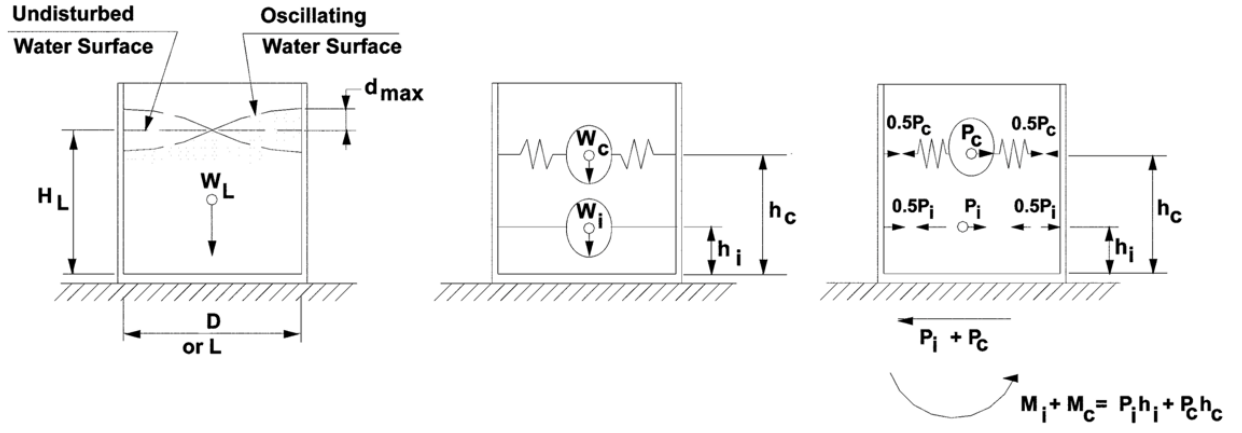

where

H_L = design depth of stored liquid
W_L = total equivalent weight of the stored liquid
D = inside diameter of circular tank
L = length of a rectangular tank
B = width of a rectangular tank
W_c = equivalent convective weight
W_i = equivalent impulsive weight
d_{max} = freeboard (sloshing height)
h_i = height of the impulsive lateral force
h_c = height of the convective lateral force
P_i = total lateral impulsive force
P_c = total lateral convective force
M_i = bending moment due to the impulsive force
M_c = bending moment due to the convective force

Fig. 8: Fluid motion in tank (a), dynamic model (b), and dynamic equilibrium of horizontal forces (c).[21,31]

As outlined in the flowchart, the first step involves calculating the impulsive and convective water masses and determining their placement within the structural model. When the ratio of water height to tank length is classified as squat ($2HL/L < 1.5$), the impulsive and convective water masses can be estimated using the following Eqs. (1)-(4):

Impulsive weight:

$$W_i = W_f \left[\frac{\tanh\left(\sqrt{3}\frac{L}{2H_L}\right)}{\sqrt{3}\frac{L}{2H_L}} \right] \quad (1)$$

Impulsive level:

$$h_i = \frac{3}{8} H_L \quad (2)$$

Convective weight:

$$W_c = W_f 0.527 \frac{L}{2H_L} \tanh\left(1.58 \frac{2H_L}{L}\right) \quad (3)$$

Convective level:

$$h_c = H_L \left[1 - \frac{\cosh\left(1.58\frac{2H_L}{L}\right) - 1}{1.58\frac{2H_L}{L}\sinh\left(1.58\frac{2H_L}{L}\right)} \right] \quad (4)$$

However, if the ratio of water height to tank length is classified as slender ($2HL/L > 1.5$), the impulsive and convective water masses are calculated using the following Eqs. (5)-(15):

Free depth:

$$\bar{H} = 1.5 \frac{L}{2} \quad (5)$$

Fixed level:

$$\hat{H} = H_L - \bar{H} \quad (6)$$

Fixed impulsive weight:

$$\hat{W}_i = \rho \hat{H} L B \quad (7)$$

Fixed impulsive level:

$$\hat{h}_i = \frac{\hat{H}}{2} \quad (8)$$

Free impulsive weight:

$$\bar{W} = \rho \bar{H} L B \quad (9)$$

Corresponding free impulsive weight:

$$\bar{W}_i = \bar{W} \left[\frac{\tanh\left(\sqrt{3}\ 0.667\right)}{\sqrt{3}\ 0.667} \right] \quad (10)$$

Free impulsive level:

$$\bar{h}_i = \frac{3}{8} 1.5 \frac{L}{2} + \hat{H} \quad (11)$$

Impulsive weight:

$$W_i = \hat{W}_i + \bar{W}_i \quad (12)$$

Impulsive level:

$$h_i = \frac{\hat{W}_i \hat{h}_i + \bar{W}_i \bar{h}_i}{W_i} \quad (13)$$

Convective weight:

$$W_c = W_f 0.527 \frac{L}{2H_L} \tanh\left(1.58 \frac{2H_L}{L}\right) \quad (14)$$

Convective level:

$$h_c = H\left[1 - \frac{\cosh\left(1.58\frac{2H_L}{L}\right)-1}{1.58\frac{2H_L}{L}\sinh\left(1.58\frac{2H_L}{L}\right)}\right] \quad (15)$$

The calculations of impulsive and convective water masses, along with their respective locations, were summarized in Table 6. The SAP2000 modeling process began by defining the impulsive and convective gap link (Step 2-3). In Step 4, the water masses were then applied, and their placement follows the calculated heights of the impulsive and convective components. The resulting model in SAP2000 was illustrated in Fig. 9.

Once the model was completed, Step 5, sinusoidal sweep wave excitation was applied as described previously. The damping used in this method follows the adjusted damping values obtained from the solid element method (Step 6). Finally, in Step 7, a nonlinear time history analysis was performed, and the results were plotted.

2.3 Additional dead load

In this method, the water contained in the tank was considered solely as an additional dead load. Table 7 summarizes the total dead load from the fluid, as well as the story dead load. The combined total load, expressed in terms of weight per square meter, was then applied in SAP2000 as a distributed load on the top floor, corresponding to the location of the water tank. The sinusoidal sweep excitation was applied. Subsequently, the damping used in this method also referred to the adjusted damping values listed in the next chapter.

Table 6: Weight and positioning of impulsive and convective parts.

W_f/W_s	Tank 1				Tank 2				Tank 3			
(%)	W_i (kgf)	h_i (cm)	W_c (kgf)	h_c (cm)	W_i (kgf)	h_i (cm)	W_c (kgf)	h_c (cm)	W_i (kgf)	h_i (cm)	W_c (kgf)	h_c (cm)
2.12	2.3	2.2	25.6	2.9	3.8	2.8	25.0	3.7	6.2	3.9	23.6	5.3
4.24	9.2	4.3	49.1	5.8	15.2	5.6	45.2	7.7	24.5	7.8	37.8	11.3
6.36	20.7	6.5	69.4	8.9	33.9	8.3	59.1	12.0	52.0	11.7	44.0	18.3
8.48	36.7	8.6	85.7	12.1	58.8	11.1	67.5	16.7	84.3	15.6	46.2	26.3
10.60	57.0	10.8	98.1	15.5	88.0	13.9	72.2	21.9	116.3	20.1	47.0	35.2
12.72	81.0	13.0	107.3	19.1	120.0	16.7	74.7	27.5	147.4	25.2	47.3	44.6

Table 7: Total fluid and story dead loads.

W_f/W_s (%)	W_f (kgf/m^2)			$W_f + W_{SDL}$ (kgf/m^2)		
	Tank 1	Tank 2	Tank 3	Tank 1	Tank 2	Tank 3
0	0.000	0.000	0.000	446.963	446.963	446.963
2.12	57.593	74.048	103.667	504.555	521.010	550.629
4.24	115.185	148.095	207.333	562.148	595.058	654.296
6.36	172.778	222.143	311.000	619.740	669.106	757.963
8.48	230.370	296.190	414.667	677.333	743.153	861.629
10.60	287.963	370.238	518.333	734.926	817.201	965.296
12.72	345.556	444.286	622.000	792.518	891.248	1068.963

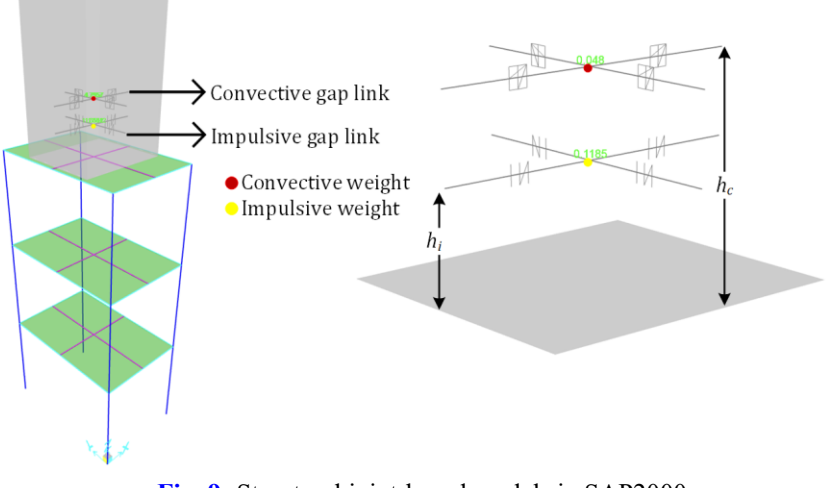

Fig. 9: Structural joint-based models in SAP2000.

3. Results and discussion

3.1 Convergence study

A convergence study was conducted to determine the optimal mesh density to be used as a reference throughout this research. As shown in Fig. 10, the convergence graph illustrates two key relationships: the number of solid elements versus the maximum structural displacement or sloshing height change (represented by the blue line), and the number of solid elements versus computational time (represented by the orange line). This analysis used Tank 1 with a fluid volume of 12.72% as the reference model. The maximum structural displacement was evaluated at a specific joint, as indicated in Fig. 11. While the maximum structural displacement produces comparable results, the sloshing water height exhibits greater variation. Accordingly, convergence can be more reliably evaluated through the maximum sloshing displacement, indicating that a mesh size of approximately 150 solid elements is sufficient for effective analysis. Increasing the mesh count beyond this threshold resulted in significantly longer computation times without substantial gains in accuracy. The final mesh configuration adopted for each model variation in SAP2000 is summarized in Table 8.

Table 8: Number of elements in mesh.

W_f/W_s (%)	Number of Elements in Mesh		
	Tank 1	Tank 2	Tank 3
2.12	192	84	112
4.24	192	84	168
6.36	140	90	144
8.48	162	126	120
10.60	162	168	150
12.72	120	210	150

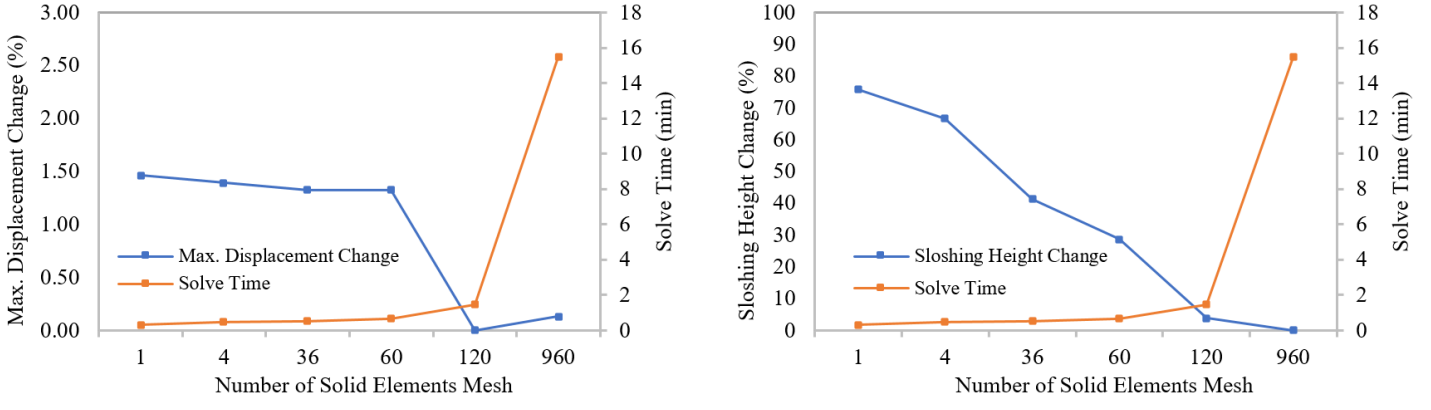

Fig. 10: Convergence study based on maximum structural displacement (a) and sloshing height (b).

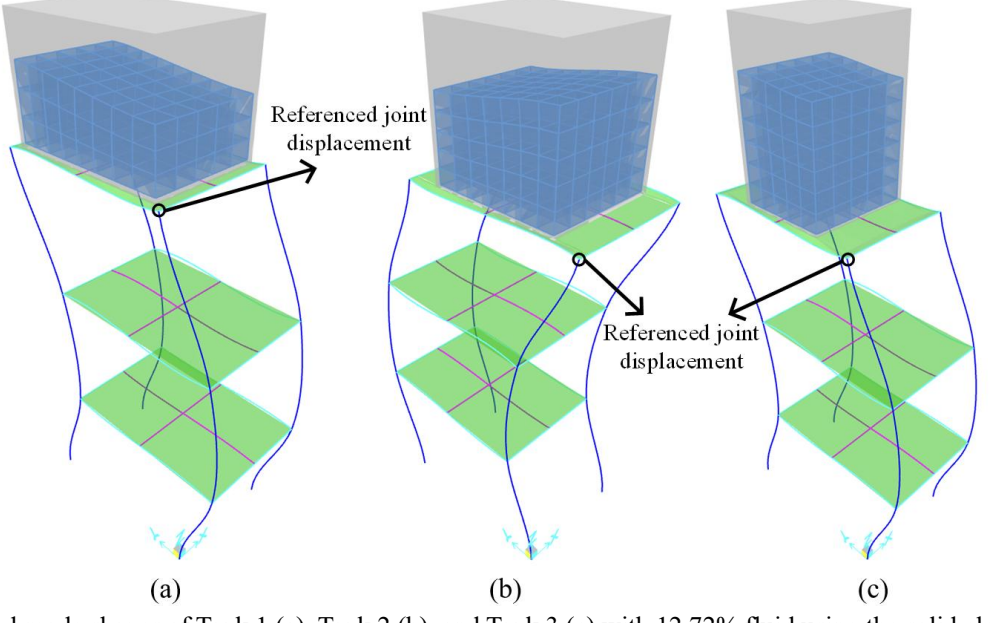

Fig. 11: Second mode shapes of Tank 1 (a), Tank 2 (b), and Tank 3 (c) with 12.72% fluid using the solid element method.

3.2 Damping assessment

The reference damping values (ξ_{ref}) were initially based on the previous experimental studies conducted by prior researcher.[25] Following the iterative process described in Steps 6 to 8 of Fig. 4, the resulting damping values are summarized in Table 9. Overall, the damping values ranged from 1.4% to 3.9% and were subsequently used as reference inputs for the other modeling approaches, including the Joint-Based and Additional Dead Load methods. The results of the structural displacement using both the reference and adjusted damping values are presented in Fig. 12 and Fig. 13. Overall, applying the reference damping values in SAP2000 using the

Table 9: Proportional damping for each model.

W_f/W_s (%)	Tank 1		Tank 2		Tank 3	
	ξ_{ref} (%)	ξ_{adj} (%)	ξ_{ref} (%)	ξ_{adj} (%)	ξ_{ref} (%)	ξ_{adj} (%)
0	0.96	1.44	0.96	1.44	0.96	1.40
2.12	1.30	2.60	1.39	2.40	1.53	2.20
4.24	1.57	3.50	1.69	2.80	1.85	2.50
6.36	1.77	3.95	1.88	3.20	1.94	2.80
8.48	1.89	3.00	1.94	3.15	1.79	2.65
10.60	1.94	3.85	1.89	3.10	1.41	2.20
12.72	1.92	3.90	1.71	3.00	0.79	1.50

Notes: ξ_{ref} = referenced damping, ξ_{adj} = adjusted damping in SAP2000 models.

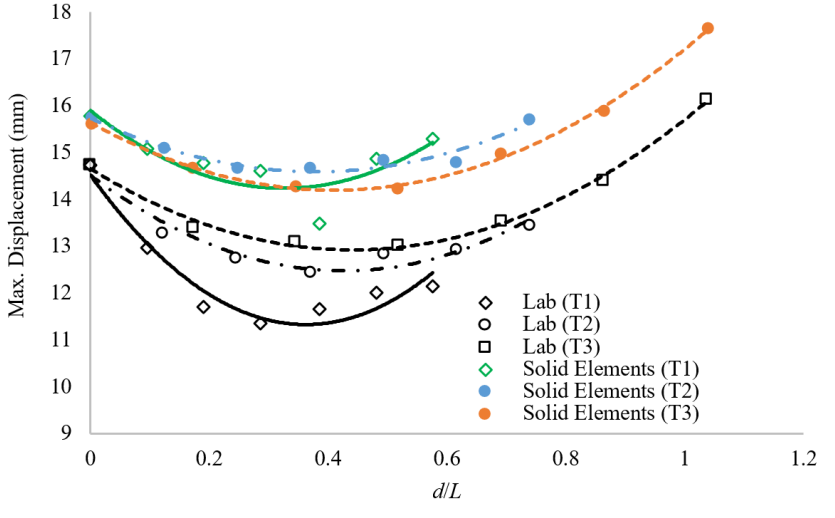

Fig. 12: Comparative study of laboratory test (Lab) and solid elements method with referenced damping for Tank 1 (T1) to Tank 3 (T3).

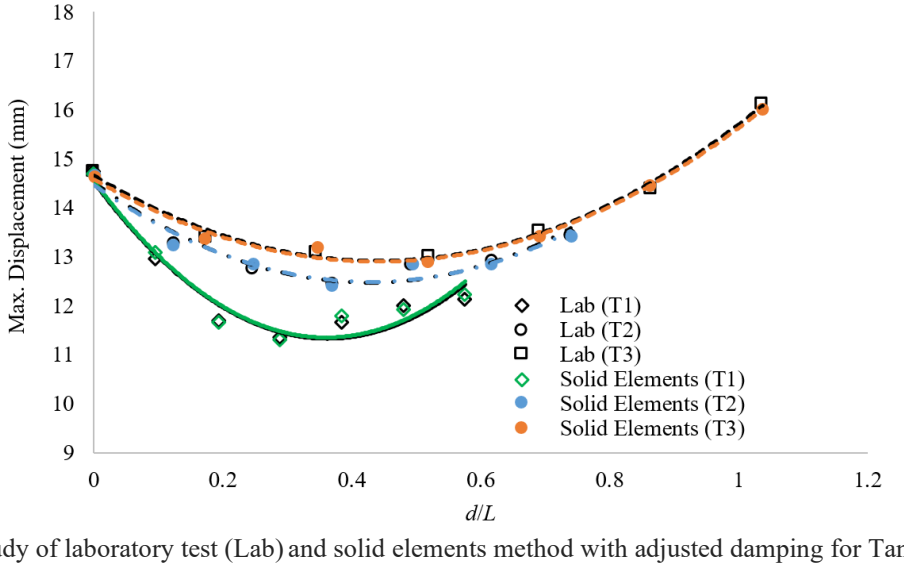

Fig. 13: Comparative study of laboratory test (Lab) and solid elements method with adjusted damping for Tank 1 (T1) to Tank 3 (T3).

solid element method yielded higher maximum displacement compared to the experimental results. This discrepancy is closely associated with the damping conditions experienced by the structure during physical testing, which were not fully known or accurately replicated in the numerical model.

3.3 Comparison of structural displacement between solid elements method and laboratory test

This section presents a comparison of structural displacement recorded over a 50-second duration during both the experimental test and software-based analysis. This study took several model variations of Tanks 1 through 3, each with different water capacities ranging from 0% to 12.72%. The selected model samples, presented in Fig. 14 to Fig. 16, demonstrate that the displacement trends prior to the onset of free vibration, as simulated using the solid elements method, closely align with those observed in the experimental results. However, the structural response behavior following the free vibration phase varied across cases. For the empty tank, the SAP2000 simulation results were more consistent and generally higher than the experimental values. In contrast, for tanks containing water, the majority of structural displacement results obtained using the solid elements method were lower than those observed in the laboratory tests. This behavior is closely related to the damping conditions experienced by the structure during testing, which were not fully known or accurately represented within the software model.

3.4 Comparison of structural displacement across modeling methods

Firstly, the joint-based method produced higher maximum displacement values than the solid element method, with an

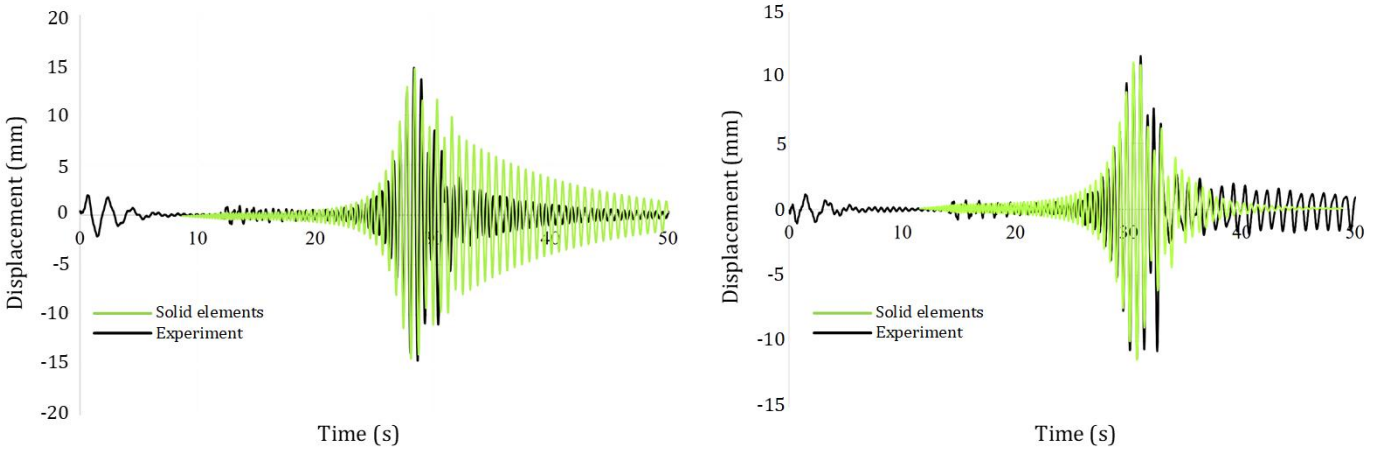

Fig. 14: Comparison of structural displacement between solid elements method and experiment for Tank 1 with W_f/W_s = 0% (a) and 8.48% (b).

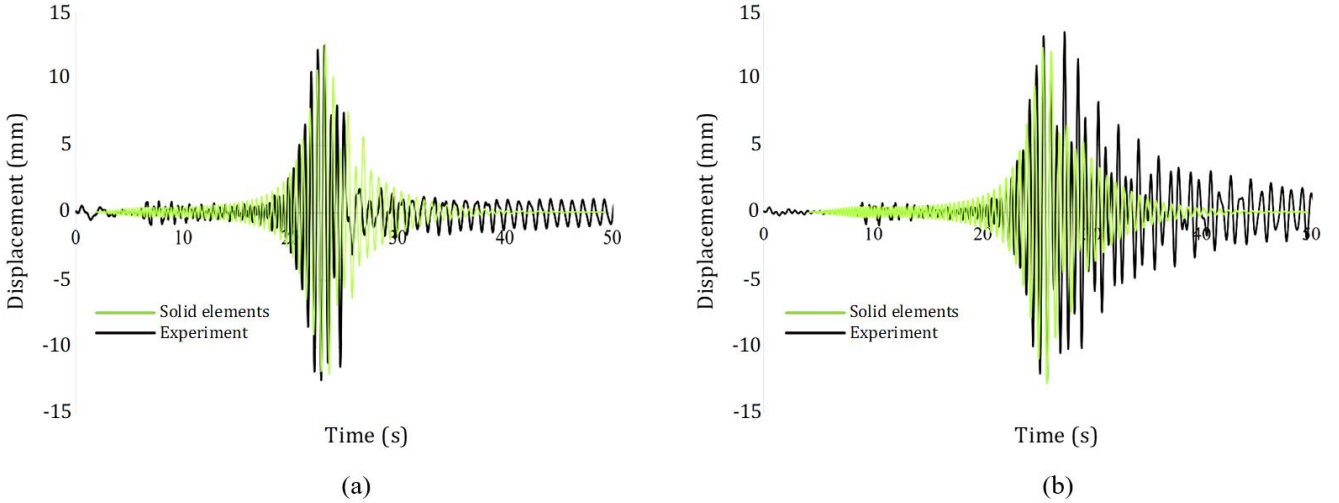

Fig. 15: Comparison of structural displacement between solid elements method and experiment for Tank 2 with Wf/Ws = 4.24% (a) and 10.60% (b).

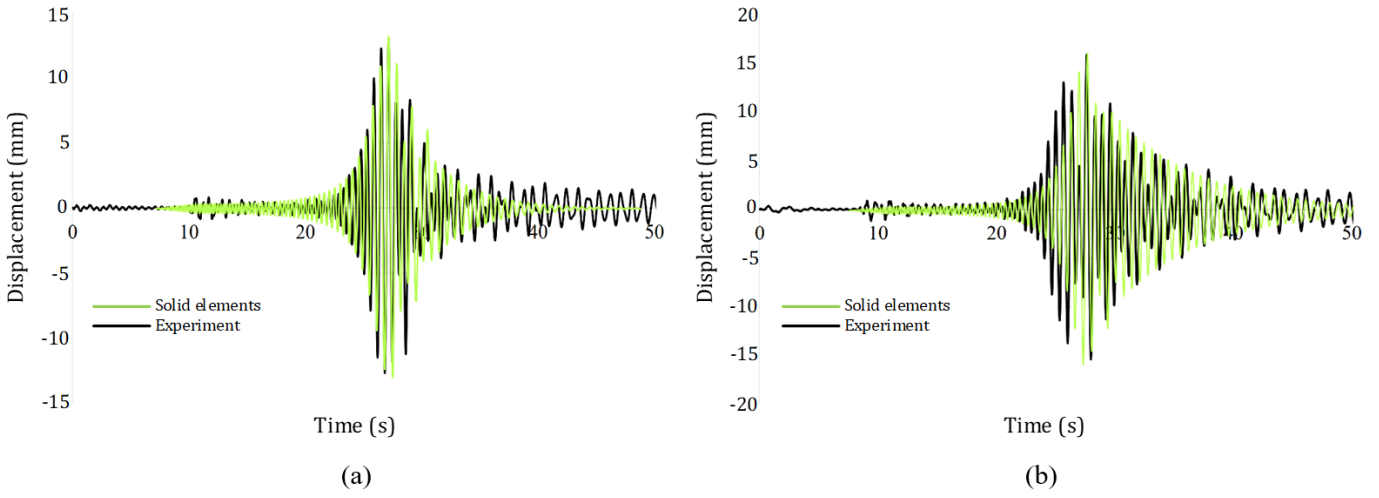

Fig. 16: Comparison of structural displacement between solid elements method and experiment for Tank 3 with W_f/W_s = 6.36% (a) and 12.72% (b).

average difference across the three tank models of approximately 13.62% (see Fig. 17 to Fig. 19.). Secondly, the additional dead load method resulted in even greater displacement values compared to both the solid element and joint-based methods. On average, the difference in maximum displacement relative to the solid element method was about 13.81%. These findings indicate that both the additional dead load and joint-based methods yield structural responses that are more conservative than the solid element method, resulting in overestimated values. Therefore, the primary advantage of employing the solid element method, which accounts for complex hydrodynamic behavior, lies in its ability to clearly visualize the sloshing effect. This, in turn, enhances design accuracy.

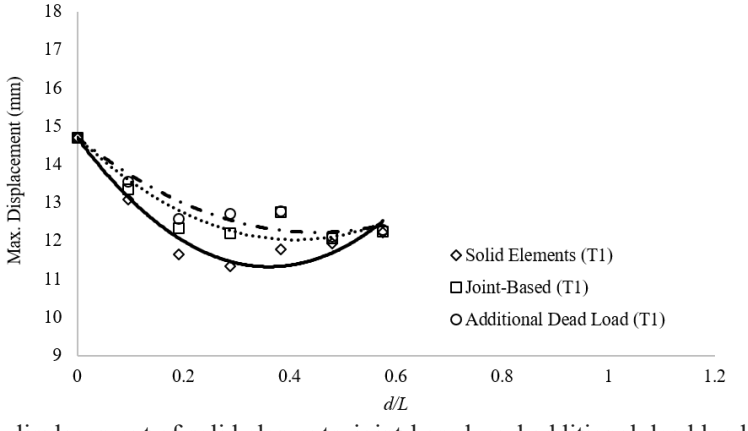

Fig. 17: Comparative displacement of solid elements, joint-based, and additional dead load methods for Tank 1.

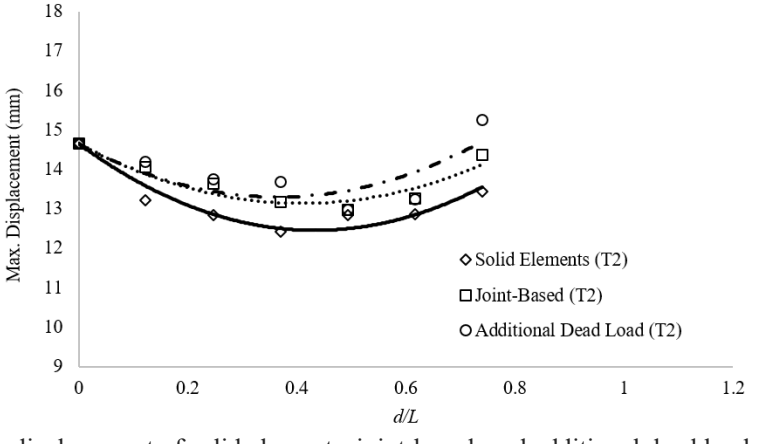

Fig. 18: Comparative displacement of solid elements, joint-based, and additional dead load methods for Tank 2.

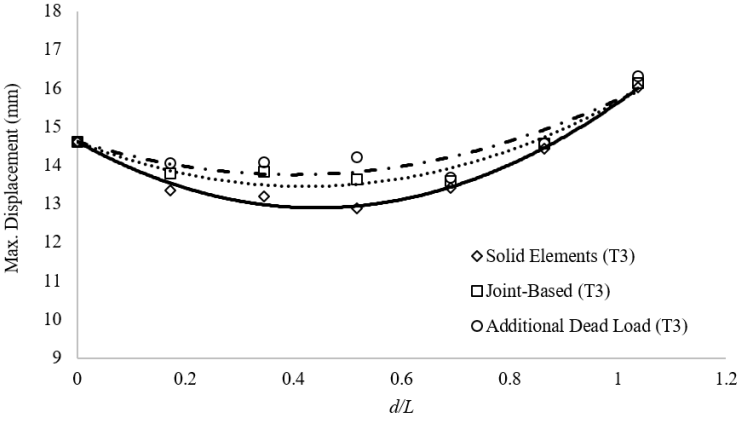

Fig. 19: Comparative displacement of solid elements, joint-based, and additional dead load methods for Tank 3.

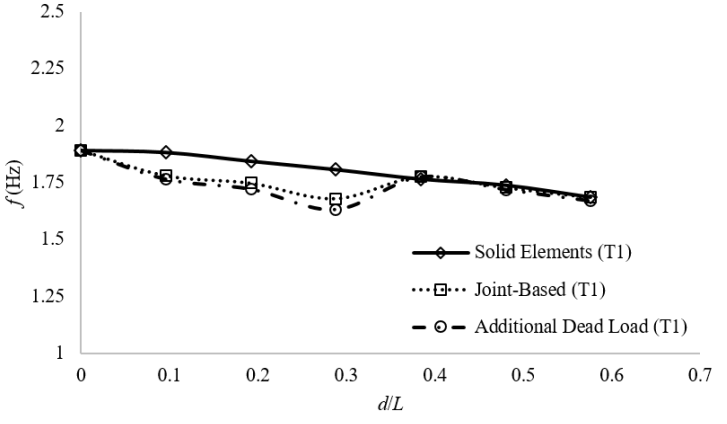

Fig. 20: Comparative natural frequency of solid elements, joint-based, and additional dead load methods for Tank 1.

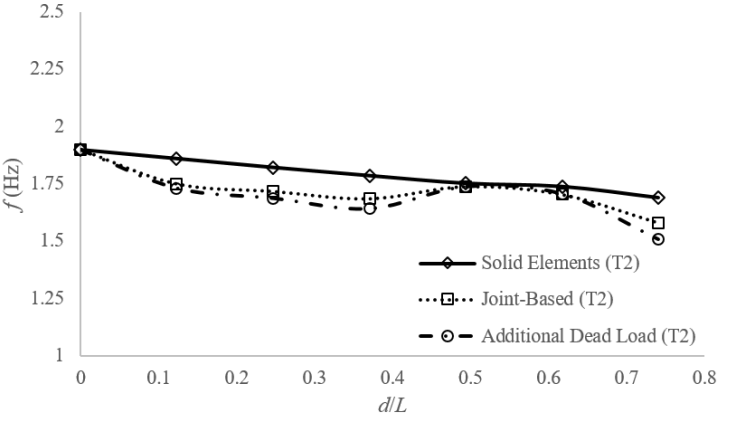

Fig. 21: Comparative natural frequency of solid elements, joint-based, and additional dead load methods for Tank 2.

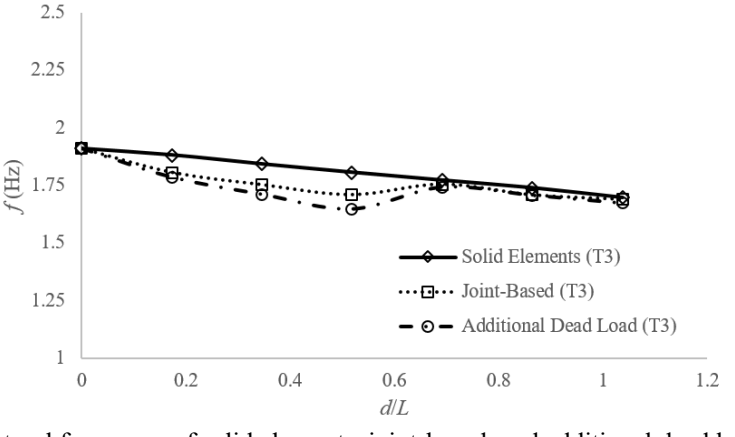

Fig. 22: Comparative natural frequency of solid elements, joint-based, and additional dead load methods for Tank 3.

3.5 Comparison of natural frequency across modeling methods

Fig. 20 to Fig. 22 illustrate the relationship between the water depth-to-tank length ratio (d/L) and the natural frequency. Consistently, an increase in d/L leads to a decrease in the natural frequency, although the reduction tends to plateau. Among the methods, the solid element approach consistently yields the highest frequency values, whereas the joint-based method produces the lowest. The additional dead load method falls between the two, generally closer to the joint-based results but slightly higher. The differences among the methods are pronounced for $d/L \leq 0.4$ but gradually diminish as d/L approaches 0.7.

3.6 Comparison of base shear across modeling methods

Overall, Fig. 23 to Fig. 25 show that base shear decreases sharply at the initial increase of d/L, then tends to stabilize or rise again at larger d/L values. The solid elements, joint-based, and additional dead load methods produce similar overall trends, with relatively small differences among them and only minor variations at certain points. In general, the additional dead load method yields slightly higher values than the other two methods at larger d/L. For Tank 1, the base shear decreases from approximately 210 kgf to about 160 kgf, followed by a slight increase at $d/L \approx 0.3$–0.4, before stabilizing. In Tank 2, the initial decrease is smoother than in Tank 1, with the base shear reducing to around 165 kgf and then increasing again for $d/L > 0.6$. Tank 3 shows a more gradual initial decrease, reaching a minimum of about 170 kgf at $d/L \approx 0.4$–0.5, followed by a significant rise to over 200 kgf when $d/L \geq 1$.

3.7 Comparison of acceleration across modeling methods

In contrast to the base shear results, the solid elements method consistently produces the highest acceleration values, likely due to the increasing influence of higher modes. The joint-based method yields the lowest values across almost the entire d/L range, while the additional dead load method lies in between, generally closer to the joint-based results. Nonetheless, the differences among the methods are relatively small, and the overall trends remain consistent. For Tank 1 as shown in Fig. 26, the maximum acceleration decreases from approximately 1.9 m/s² to about 1.2 m/s². In Tank 2 (see Fig. 27), the initial reduction is more gradual, from 1.9 m/s² to around 1.2-1.3 m/s², with an almost flat trend for $d/L > 0.4$. Tank 3 shows a similar pattern to Tank 2 as depicted in Fig. 28; however, after reaching its minimum at $d/L \approx 0.5$-0.6, the acceleration increases again, reaching over 1.6 m/s² at $d/L \approx 1.2$.

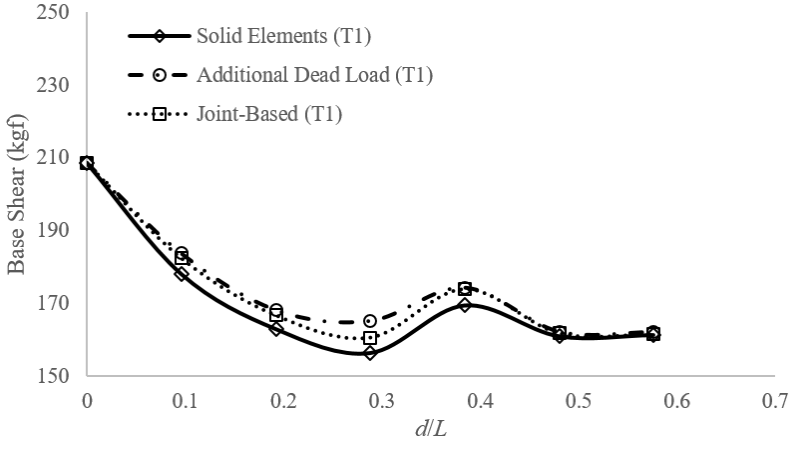

Fig. 23: Comparative base shear of solid elements, joint-based, and additional dead load methods for Tank 1.

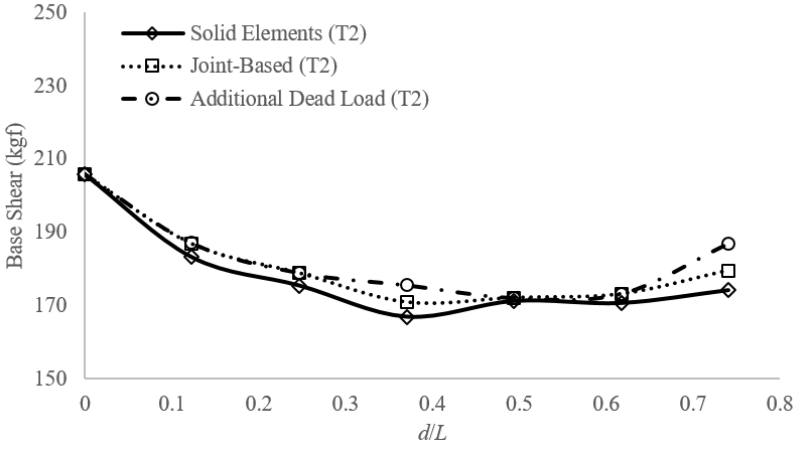

Fig. 24: Comparative base shear of solid elements, joint-based, and additional dead load methods for Tank 2.

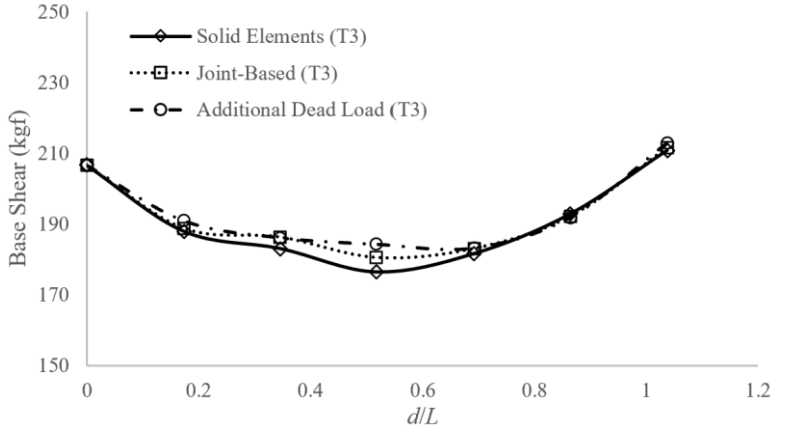

Fig. 25: Comparative base shear of solid elements, joint-based, and additional dead load methods for Tank 3.

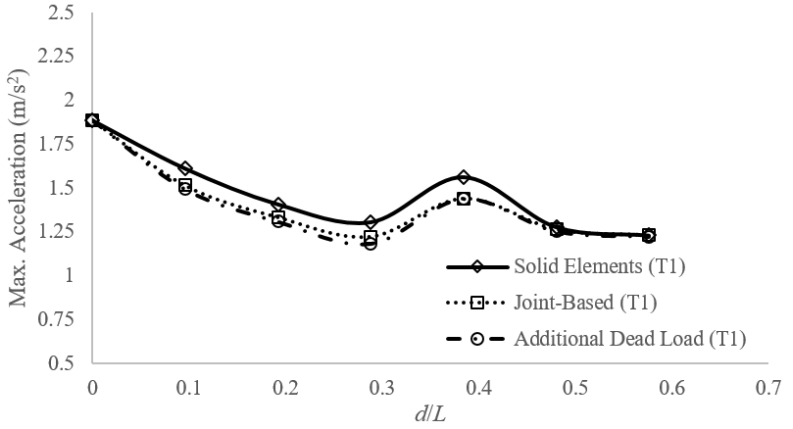

Fig. 26: Comparative acceleration of solid elements, joint-based, and additional dead load methods for Tank 1.

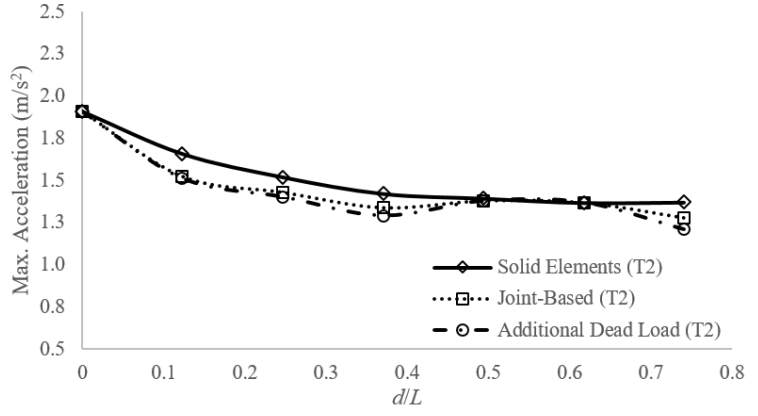

Fig. 27: Comparative acceleration of solid elements, joint-based, and additional dead load methods for Tank 2.

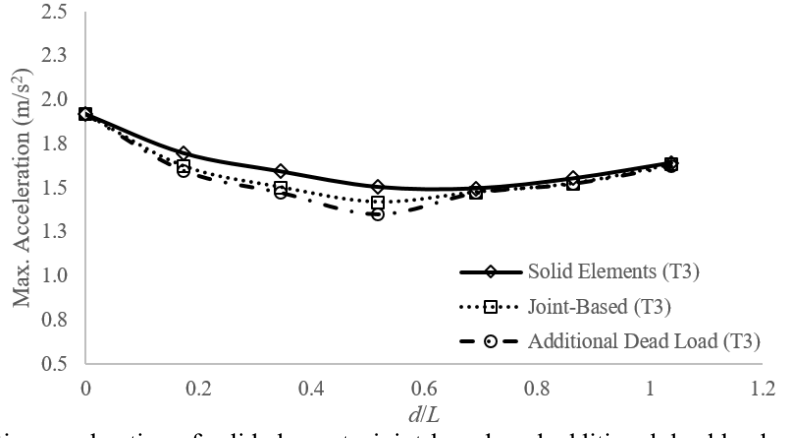

Fig. 28: Comparative acceleration of solid elements, joint-based, and additional dead load methods for Tank 3.

4. Conclusion

This study yields several key conclusions derived from each main stage, encompassing the physical test model, structural modeling, and analytical results:

a) Structural Model

The structural model used in this research was based on a previous experimental study involving a three-story steel frame structure with a water tank positioned on the top floor. Three variations of tank dimensions were analyzed, each with seven different water depths.

b) Modeling Approach

Fluid–Structure Interaction (FSI) was modeled using SAP2000. The solid elements method effectively captured the explicit behavior of FSI, including sloshing effects through the use of gap link that connect water to the tank walls. In the joint-based method, gap links were utilized to represent the impulsive and convective components of the fluid mass. The additional dead load method models the fluid as a static load, without capturing dynamic interaction.

c) Convergence Study

The optimal number of solid elements meshes was around 150. Increasing the mesh beyond this number was found to be inefficient, as it extended computation time without significantly improving accuracy.

d) Damping Implementation

Applying reference damping values in the solid element model resulted in larger maximum displacements compared to experimental results. Adjusted damping values ranging between 1.4% and 3.9% were found to be more representative and were subsequently used across all modeling approaches.

e) Structural Displacement

In solid elements method, the structural displacement trends closely matched those observed in the experiment. However, during the free vibration phase, SAP2000 results tended to underestimate displacements compared to experimental data, likely due to unmodeled damping effects. By contrast, the joint-based approach yielded higher maximum displacements than the solid element method, with an average deviation of 13.62%. The additional dead load method produced the highest displacement values among the three, with an average deviation of 13.81% compared to the solid element method

f) Natural Frequency

All three methods exhibit a consistent trend in which the natural frequency decreases with increasing d/L. The solid elements method provides the highest frequency estimates, whereas the joint-based method yields the lowest. The differences among the methods become less pronounced at larger d/L values, particularly for Tank 3.

g) Base Shear

The minimum base shear occurs at $d/L \approx 0.3$–0.5, followed by an increasing trend at higher water depths. Tank 3 exhibits the most significant rise at larger d/L values, whereas Tanks 1 and 2 remain relatively more stable. Overall, the solid elements method produces the lowest base shear compared to the other methods.

h) Acceleration

The solid elements method gives the highest acceleration values, likely because higher modes have more influence. The joint-based method gives the lowest values across most of the d/L range, while the additional dead load method falls in between, closer to the Joint-Based results. Overall, the differences are small, and the trends are consistent.

Acknowledgments

The first author extends sincere appreciation to the Faculty of Engineering at Gadjah Mada University, Indonesia, for providing scholarship support for the PhD degree program related to this research. The research has also greatly benefited from the assistance of Computers and Structures Inc. (CSI) America, which supplied the licensed SAP2000 software and a high-performance hardware used in the analysis. The authors would like to thank the late Dr. Teddy Boen for giving opportunities and funding to conduct research at the CSI America headquarters in Walnut Creek, California, USA in 2022. Moreover, the authors deeply appreciate the support and contributions from the CSI America team, including Ashraf Habibullah, Syed Hasanain, Faisal Habib, Riaz Syed, Umer Haroon, Bob Morris, and teams. The Open Access Charge of this research publication was fully funded by CSI America.

Conflict of Interest

There is no conflict of interest.

Supporting Information

Not applicable.

CRediT Statement

Sarah Eden Suryanto: Conceptualization, Resources, Data Curation, Methodology, Project administration, Investigation, Formal analysis, Writing – Original draft, Writing – Review & editing, Visualization. **Iman Satyarno**: Conceptualization, Methodology, Writing – Review, Supervision. **Bambang Supriyadi**: Supervision. **Ashar Saputra**: Supervision.

References

[1] K. Shahzada, U. Ahmad Noor, Z. Xu, In the wake of the March 28, 2025 Myanmar earthquake: a detailed examination, *Journal of Dynamic Disasters*, 2025, **1**, 100017, doi: 10.1016/j.jdd.2025.100017.

[2] R. Enokida, Y. Fukushima, C. Tang, T. Pan, C. Kuo, K. Ikago, T. Izumi, S. Kuriyama, Earthquake disaster resilience in Taiwan

observed from the April 2024 ML 7.1 Hualien earthquake, *Frontiers in Built Environment*, 2025, **11**, 1593942, doi: 10.3389/fbuil.2025.1593942.

[3] M. W. Andaya, R. Grutas, S. Tsuno, H. Yamanaka, Estimation of high-rise building response in metro Manila, Philippines, during the 2019 central Luzon earthquake based on video data analysis, *Earthquake Spectra*, 2025, 87552930251353814, doi: 10.1177/87552930251353814.

[4] K. He, H. Zhu, J. Ye, An integrated model for fluid-structure-seabed interaction based on SPH-FEM: Validation and a practical engineering application, *Ocean Engineering*, 2024, **313**, 119636, doi: 10.1016/j.oceaneng.2024.119636.

[5] M. R. I. Islam, SPH-based framework for modelling fluid–structure interaction problems with finite deformation and fracturing, *Ocean Engineering*, 2024, **294**, 116722, doi: 10.1016/j.oceaneng.2024.116722.

[6] K. C. Ng, W. C. Low, H. Chen, A. Tafuni, A. Nakayama, A three-dimensional fluid-structure interaction model based on SPH and lattice-spring method for simulating complex hydroelastic problems, *Ocean Engineering*, 2022, **260**, 112026, doi: 10.1016/j.oceaneng.2022.112026.

[7] Y. Shimizu, A. Khayyer, H. Gotoh, An implicit SPH-based structure model for accurate Fluid–Structure Interaction simulations with hourglass control scheme, *European Journal of Mechanics - B/Fluids*, 2022, **96**, 122-145, doi: 10.1016/j.euromechflu.2022.07.007.

[8] Z. Yu, X. Yao, D. Chen, Q. Ma, X. Lyu, D. Huang, Numerical implementation of an extended multi-resolution SPH-PD coupling model for fluid-structure interaction problem with impacting failure, *Applied Ocean Research*, 2024, **150**, 104121, doi: 10.1016/j.apor.2024.104121.

[9] Y. Ramdani, H. Priyosulistyo, D. Sulistyo and R. Triatmadja, The Damping Properties of A Steel Structural Model with A Box-Shaped Water Reservoir upon Top Floor, *International Journal of GEOMATE,* 2023, **24**, 33-42, doi: 10.21660/2023.101.3633.

[10] D. Kalliontzis, Arbitrary Lagrangian-Eulerian formulation with Skeleton-based Structural Models (ALE-SSM) framework for water-structure interaction with large structural deformations, *International Journal of Multiphase Flow*, 2025, **189**, 105269, doi: 10.1016/j.ijmultiphaseflow.2025.105269.

[11] Y. Li, Y. Qu, F. Xie, G. Meng, An arbitrary Lagrangian-Eulerian method for nonlinear structural-acoustic interaction of hyperelastic solid and compressible viscous fluid, *Journal of Computational Physics*, 2022, **471**, 111665, doi: 10.1016/j.jcp.2022.111665.

[12] Z. Qian, L. Wang, C. Zhang, Q. Chen, A highly efficient and accurate Lagrangian–Eulerian stabilized collocation method (LESCM) for the fluid–rigid body interaction problems with free surface flow, *Computer Methods in Applied Mechanics and Engineering*, 2022, **398**, 115238, doi: 10.1016/j.cma.2022.115238.

[13] P. Sun, J. Xu, L. Zhang, Full Eulerian finite element method of a phase field model for fluid–structure interaction problem, *Computers & Fluids*, 2014, **90**, 1-8, doi: 10.1016/j.compfluid.2013.11.010.

[14] M. Zhu, M. H. Scott, Modeling fluid–structure interaction by the particle finite element method in OpenSees, *Computers & Structures*, 2014, **132**, 12-21, doi: 10.1016/j.compstruc.2013.11.002.

[15] T. Novo, H. Varum, F. Teixeira-Dias, H. Rodrigues, M. F. Silva, A. C. Costa, L. Guerreiro, Tuned liquid dampers simulation for earthquake response control of buildings, *Bulletin of Earthquake Engineering*, 2014, **12**, 1007-1024, doi: 10.1007/s10518-013-9528-2.

[16] N. R. C. Tuasikal, Analysis of the Effect of Roof-Top Swimming Pool Position on the Effectiveness of Tuned Liquid Dampers in Reducing Seismic Response in Earthquake-Resistant Buildings (Case Study: Hotel in Yogyakarta, Indonesia), Gadjah Mada University, Yoyakarta, 2024.

[17] X. Hu, Z. Zhao, D. Weng, D. Hu, Design of a pair of isolated tuned liquid dampers (ITLDs) and application in multi-degree-of-freedom structures, *International Journal of Mechanical Sciences*, 2022, **217**, 107027, doi: 10.1016/j.ijmecsci.2021.107027.

[18] G. Z. Putri, H. D. Setio, The Effect of Viscosity Variations in a Rectangular Water Tank Tuned Liquid Damper on the Structural Dynamic Response (in Indonesian: Pengaruh Variasi Viskositas Pada Rectangular Water Tank Tuned Liquid Damper Terhadap Respons Dinamik Struktur, *6th Andalas Civil Engineering (ACE) Conference*, Padang, October, 2019.

[19] Z. Zhao, R. Zhang, Y. Jiang, C. Pan, A tuned liquid inerter system for vibration control, *International Journal of Mechanical Sciences*, 2019, **164**, 105171, doi: 10.1016/j.ijmecsci.2019.105171.

[20] P. K. Malhotra, T. Wenk, M. Wieland, Simple procedure for seismic analysis of liquid-storage tanks, *Structural Engineering International*, 2000, **10**, 197-201, doi: 10.2749/101686600780481509.

[21] ACI Committee, *Seismic Design of Liquid-Containing Concrete Structures and Commentary (ACI 350.3-20)*, American Concrete Institute, USA, 2020.

[22] K. Meskouris, Structural Dynamics Models, Methods, Examples, Ernst & Sohn, Berlin, 2000, ISBN: 3433013276.

[23] J. T. C. Basañez, R. I. B. Canales, R. J. B. Cartalla, C. D. A. Lumod, D. B. J. Tolibas and R. M. F. Yan, A Thesis of Tuned Liquid Damper Design of A 40-Storey RC Structure, Cebu Institute of Technology University, Cebu, 2019.

[24] E. L. Wilson, Chapter 23: Fluid-Structure Interaction, *Three Dimensional Static and Dynamic Analysis of Structures*,

Computers and Structures, Inc., Berkeley, 2000, ISBN: 0923907009 .
[25] Y. Ramdani, Tuned Liquid Damping System on Steel Frame Structures (in Indonesian: Sistem Peredam Cairan Terkendali (Tuned Liquid Damping) pada Struktur Portal Baja), Gadjah Mada University, Yogyakarta, 2023.
[26] A. Mieses, Modeling fluid-structure interaction, Wiki Technical Knowledge Base of Computers and Structures Inc., California, 2017.
[27] CSI America, SAP2000 Structural Analysis and Design - CSI Analysis Reference Manual, Computers and Structures Inc., California, 2017.
[28] N. H. Cook, R. R. Archer, S. H. Crandall, N. C. Dahl, F. A. McClintock, E. Rabinowicz and G. S. Reichenbach, An Introduction to the Mechanics of Solids, 1st ed., McGraw-Hill Book Company Inc., New York – Toronto – London, 1959.
[29] R. D. Cook and W. C. Young, Advanced Mechanics of Materials, 1st ed., Macmillan Publishing Company, New York, 1985, ISBN: 0133969614.
[30] S. Timoshenko and J. N. Goodier, Theory of Elasticity, 2nd ed., McGraw-Hill Book Company Inc., New York – Toronto – London, 1951.
[31] G. W. Housner, The dynamic behavior of water tanks, *Bulletin of the Seismological Society of America*, 1963, **53**, 381-387, doi: 10.1785/bssa0530020381.